Effectiveness of high-frequency ELM pacing with deuterium and non-fuel pellets in DIII-D

A. Bortolon[1], L.R. Baylor[2], R. Maingi[1], D.K. Mansfield[1], A.L. Roquemore[1], R. Lunsford[1], A. Nagy[1], M.Vorenkamp[1], I. Bykov[3], G.L. Jackson[4], R.A Moyer[3], T. Osborne[4], N. Commaux[2], D. Shiraki[2], C.J. Lasnier[5], M.J. Makowski[5], P.B. Parks[4], R. Groebner[4], R. Nazikian[1] and the DIII-D team

[1] Princeton Plasma Physics Laboratory, 100 Stellarator Rd, Princeton, NJ 08540 USA
[2] Oak Ridge National Laboratories, PO Box 2008, Oak Ridge TN 37831, USA
[3] University of California San Diego, 9500 Gilman Dr, La Jolla, CA 92093, USA.
[4] General Atomics, 3550 General Atomics Ct, San Diego CA 92121, USA
[5] Lawrence Livermore National Laboratory, 7000 East Ave, Livermore CA 94551, USA

E-mail contact of main author: abortolon@pppl.gov

Abstract. DIII-D studies of high-frequency ELM pacing by pellet injection were extended to ITER scenarios at low neutral beam torque and to the use of non-fuel materials, a technique that could potentially reduce the throughput to the pumping and fuel reprocessing systems. ELM peak heat flux mitigation was obtained with injection of D_2 pellets at frequencies up to 90 Hz in low-torque ITER baseline scenario (IBS, q_{95}=3.2, β_N=1.7, $n_{e,ped}$=7.5x10^{19} m^{-3}, T_{inj}<0.1 N-m). D_2 pellet injection resulted in ELM pacing at frequencies 6-8x the natural ELM frequency (10 Hz). The resulting inner divertor peak heat flux was reduced by more than a factor of 10, with minor modification in the heat-flux footprint width. However, at the highest injection frequencies, changes of the pedestal parameters similar to gas puffing were observed, resulting in a 20% reduction of pedestal pressure. The feasibility of ELM pacing with non-fuel pellets was explored with the new Impurity Granule Injector, capable of injecting sub-millimeter granules of non-fuel materials (e.g. Li, C, B_4C), at frequencies up to 200 Hz, with controllable speed (50-150 m/s) and selectable granule size. Experiments with Li granules 0.4-0.9 mm injected in plasmas at q_{95}~4.6, $n_{e,ped}$~4x10^{19} m^{-3}, β_N=1.5 demonstrated full-shot ELM pacing, with a 3-5x increase of f_{ELM} over the natural ELM frequency, and a reduction of ELM peak heat flux ~1/f_{ELM}. However, in the lower q_{95}~3.2, low-torque IBS, ELM pacing by Li granule injection did not translate into heat flux mitigation, with a fraction of paced ELMs showing peak heat flux similar to natural ELMs. The combined dataset provides a unique contribution to ELM control research, challenging the understanding of the relation between high frequency ELM pacing and heat flux mitigation.

1. Introduction

The development and validation of techniques to mitigate edge localized modes (ELM) is a primary research thrust for ITER, since transient heat flux from large type-I ELMs can potentially cause melting and cracking of the divertor target plates [1]. High frequency pacing of ELMs by on-demand triggering is a well-established ELM control technique [2, 3], but further investigations are needed to ensure sufficient and reliable ELM mitigation in ITER, where pacing of ELMs at frequencies up to 30X the natural ELM frequency is projected [4].

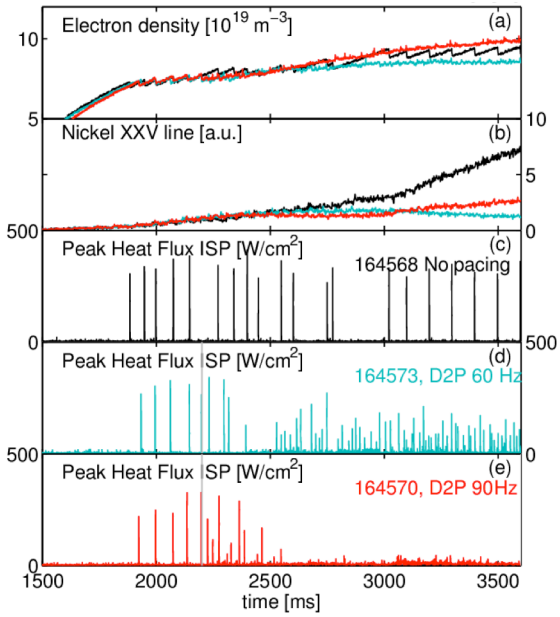

FIG. 1. Selected traces for three discharges with natural uncontrolled ELMs, D2P pacing at 60 and 90 Hz.

This motivated recent DIII-D experiments extending the study of ELM pacing and mitigation to unprecedented injection frequencies in ITER relevant operational scenarios. To that end, the deuterium pellet injection system (D2P) was configured to deliver ELM-pacing size pellets at rates up to 90 Hz. Even higher frequencies, up to 200 Hz, have been tested by non-fuel granule injection using the impurity granule injector (IGI) [5, 6], recently upgraded to allow injection of Li, C and B_4C. The use of non-fuel materials to trigger and pace ELMs has a double interest. First, in ITER the steady-state gas throughput in the vessel is limited by the capacity of pumping and fuel-processing systems. Available estimates indicate the amount of D_2 needed to inject for ELM control can be a significant fraction of the total capacity, potentially interfering with the operation of other systems, e.g. detachment control in long pulse operation [1]. The use of non-fuel pellets, in particular from low Z, non-recycling materials, e.g. Beryllium, might alleviate the issue, if the resulting dust is itself not problematic. Second, using a variety of materials, allows probing the physics of ELM triggering, given that different ablation characteristics result in different penetration depth, and particle deposition profiles.

DIII-D experiments discussed in this work were performed in the ITER baseline scenario (β_N=1.7, q_{95}=3.2) [7]. Given the important role played by plasma rotation in stability and confinement, an effort was made to operate at levels of applied torque close to the equivalent torque conditions predicted in ITER (T_{inj}~0.5 N-m). Specifically, the applied torque was varied from T_{inj}~3.5 N-m, down to 0.05 N-m by means of balanced neutral beam injection (NBI) in the co and counter current direction. In the experiments, β_N was maintained approximately constant at 1.7, by real-time adjustment of the beam input power. The divertor pumping was optimized by positioning the outer strike point (OSP) at the entrance of the cryo-pump baffle, which, unfortunately, prevents the thermography measurement of heat flux profile at the OSP. The inner strike point (ISP) sat on the central column and was typically detached between ELMs.

2. D2P Injection in IBS at Low Torque

For the experiment, the D_2 pellet injector was configured with three separate guns, each providing up to 30 Hz injection, for potential pacing frequencies up to 90 Hz. The nominal pellet size in each injector was 1.3x0.9 mm (length x diameter), for an average content of $7x10^{19}$ electrons and equivalent to 0.13 Pa-m^3 of D_2 gas. The pellets were injected at 150 m/s on a radial horizontal trajectory from the LFS 10 cm above the midplane. The measured penetration depth, which is consistent with modeling, is ~3 cm for the nominal size pellet, which reaches the top of the pedestal. Figure 1 shows the discharge evolution for a non-pellet case (164568) in this scenario with T_{inj}=0.05 N-m and P_{inj}~4 MW, just above the L-H threshold. The natural ELM frequency of uncontrolled ELMs was f_{ELM}~10 Hz, and the inner strike point peak heat flux (q_{peak}) was ~340 W/cm^2. Due to this low ELM frequency, intrinsic

metal impurities accumulated in the core, as indicated by the intensity of the Ni XXV line in the core plasma, which ramped during the discharge. The same discharge was repeated with D_2 pellet injection at 60 Hz (164573), and 90 Hz (164570). In both cases the injection started at t=2.2 s, and continued at a constant rate to the end of the current flat top. With the start of D_2 pellet injection, the ELM frequency increased and divertor peak heat flux measured at the inner strike-point decreased to low levels, maintained until the end of the D2P injection or, for 90 Hz case, the onset of strong MHD activity at t=3.6 s. In both cases, the Ni accumulation was strongly reduced by the application of the pellets as has been observed in previous experiments [8, 6].

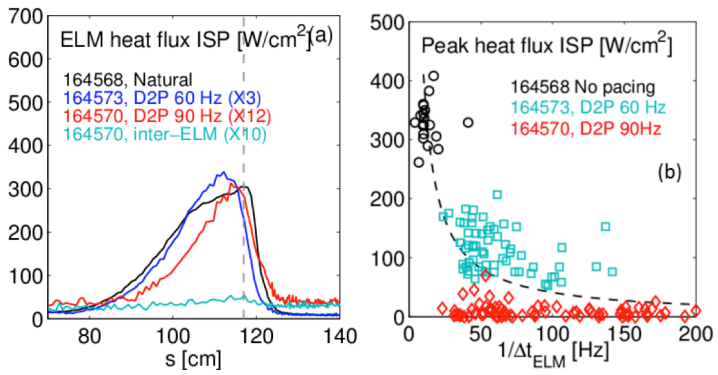

FIG. 2. (a) Selected heat flux profiles from the ISP. (b) Distribution of ELM q_{peak} as a function of inter-ELM period.

During D_2 ELM pacing at 60 Hz, clear ELMs, with reduced q_{peak}~80-130 W/cm maintained a plasma density lower than the reference discharge, as expected if ELMs are triggered before the pedestal density increases up to instability. For 90 Hz D2P injection, paced ELMs are characterized by q_{peak}~5-20 W/cm^2, i.e. 90-95% smaller than natural ELMs. In this case the density is observed to increase and exceed the values of the reference discharge; however individual pellets are not observed to increase the density. The higher divertor D_α baseline emission [see Fig. 3(a)] and a 40-50% increase of radiated power from the divertor (not shown), both indicate increased recycling and higher density of neutrals, which provide fueling across the separatrix.

Figure 2(a) compares the poloidal profile of heat flux measured across a natural ELM from the reference discharge and two triggered ELMs from the D2P discharges. The profiles for paced ELMs are scaled to the natural ELM amplitude to allow a comparison of the footprint. While no significant change in the footprint shape is observed at 60 Hz pacing, for 90 Hz pacing a 20% reduction of the footprint width is found. Notice that the inter-ELM profile, with q_{peak}<5 W/cm^2 is close to the noise level and does not show significant features, indicating detachment of the ISP.

The dependence of mitigation strength on ELM frequency is shown in Figure 2(b), for the discharges considered, with ELMs in the time interval 2.5-3.6 s, where q_{peak} for each ELM is plotted as a function of the "instantaneous" ELM frequency, defined as the inverse of pre-ELM period Δt_{ELM}, i.e. the time since the previous ELM crash. Notice that, while the nominal injection frequency determined by the injectors operation was constant during the interval analyzed, a broad range of the injection/ELM frequencies is found. The spread is associated with the range of variability of firing times, pellet mass, injection velocity, etc. The figures also include the expectation from $1/f_{ELM}$ scaling of q_{peak}, normalized to fit the reference discharge data. For 60 Hz injection q_{peak} appears to decrease with smaller pre-ELM periods, but the values observed exceed the $1/f_{ELM}$ expectation. A significant spread ~100 W/cm2 is observed for q_{peak}, which, for paced ELMs with similar $\Delta t_{ELM,}$ can vary within a factor of two. In the case of 90 Hz, where injections as close as 5 ms are found, q_{peak} is found not to depend significantly on the pre-ELM period, resulting in much lower than the $1/f_{ELM}$ scaling at all frequencies. These observations suggest that the nature of the small ELM events resulting from 90 Hz D_2 injection to be different than for natural and 60 Hz paced ELMs.

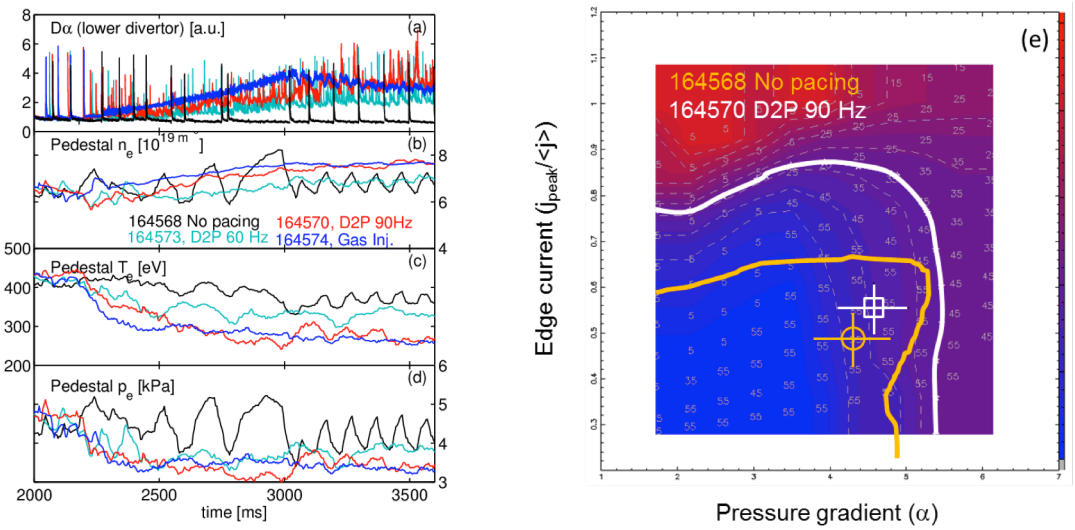

FIG. 3. Left: evolution D_α emission from lower divertor, n_e, T_e and p_e at the top of the pedestal. Right: peeling-ballooning stability diagram for 90Hz D2P injection. The yellow marker and line indicate the working point and stability boundary for the reference case with uncontrolled ELMs.

In this regard it is interesting to consider the evolution of the pedestal parameters during different levels of D_2 injection (Figure. 3). The start of D_2 injection is accompanied by a 2-3X increase of D_α emission baseline from the OSP, indicating stronger recycling and more neutrals in the divertor region. The pedestal density $n_{e,ped}$~$6x10^{19}$ m^{-3} for 60 Hz is similar to the reference discharge, but increases up to ~$7.5x10^{19}$ m^{-3} for the 90 Hz pacing. At the same time $T_{e,ped}$ decreases from 400 to 300 eV, due to the cooling effect from pellet ablation and the additional neutral fueling. As a result the pedestal electron pressure during high frequency pellet injection decreased by ~20% from the non-pellet reference, from average values of 4.2 kPa to 3.4 kPa. Figure 3 also includes traces from discharge 164574, where D2P injection was substituted by gas injection at a rate nominally equivalent to 90 Hz D2P (130 mbar-L/s). Interestingly, in this case, pedestal parameters evolved to values very similar to the 90 Hz pacing discharge. Similarly, the D_α emission shows an increase of the baseline and absence of spikes, suggesting that the conditions for a pedestal condition stable to type-I ELMs had been found. Linear MHD simulations with the ELITE code [9] have been performed to investigate the stability of the peeling-ballooning (P-B) modes in the pedestal conditions of the high frequency D2P. Figure 3(e) shows the P-B stability diagram, for the case of 90 Hz D2P. Compared to the reference non-pellet large ELM discharge, the stability boundary is found at larger values of bootstrap current j_{BS} and the normalized pedestal pressure gradient α.

The results indicate an improved stability of the pedestal under the high recycling conditions found at the largest injection frequencies tested, which is consistent with the absence of type-I ELMs in the matching gas-fuelled discharge, with similar pedestal parameters.

3. ELM Pacing with Non-fuel Granule Injection

Previous results in non-ITER scenarios with Li injection showed that effective ELM pacing and mitigation can be obtained with non-fuel granules [6]. By injecting with Li spheres (0.3-1.0 mm) in plasmas at q_{95}=4.6, β_N =1.5 and moderate torque of 3.0 N-m, ELM pacing was demonstrated for the full discharge length, with constant $H_{98y,2}$≈1.2, effective density control and reduced high-Z impurities. In this scenario the ELM frequency was increased by 3-5x over the natural ELM frequency (12 Hz), but the maximum ELM frequency appeared to be limited only by the injection frequency of the larger granules.

These early results motivated an upgrade of the IGI, now capable to inject other non-fuel materials in granular form to explore the physics of granule ablation and effects on plasma performance, in view of a possible use of beryllium in next-step devices. In particular, recent ELM pacing experiments in the IBS, have included injection of lithium spheres (0.7 mm diameter), vitreous carbon spheres (0.4, 0.6 mm) and boron carbide grit (B_4C, irregular shape, variable size 0.2-0.7 mm). The dynamics of granule ablation was investigated through fast-imaging frame rates of 10-20 kHz, sufficient to resolve ablation events, generally lasting 0.5-1.5 ms (Fig. 4).

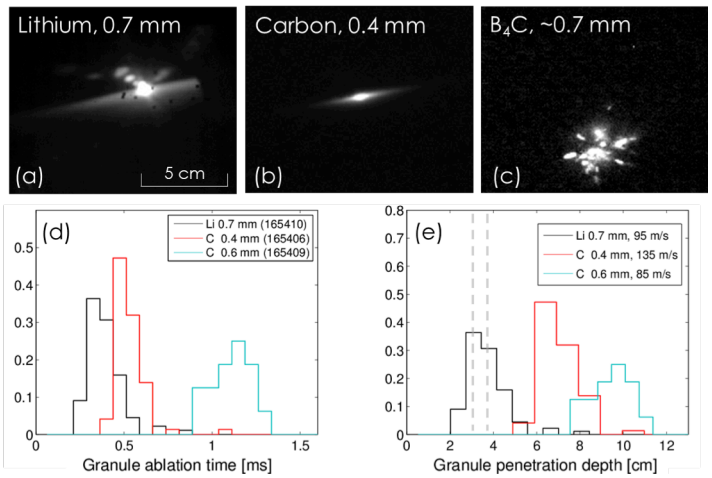

FIG. 4. (a,b,c) Fast camera frames showing ablation of granules of different materials tested, with relative distributions of measured ablation time (d) and penetration depth (e). The vertical dashed lines indicate the pedestal top location.

Ablation of Li and C spheres takes place in a similar fashion, with elongated, field aligned emission, likely from first ionization charge states, extending by <1 cm in the direction normal to the field. In contrast, most of B_4C granules appear to shatter upon contact with the plasma boundary, a behavior likely associated with the non-spherical shape, characterized by sharp edges. Figure 4(e) shows the distribution of granule penetration depths, inferred combining the total ablation times and the measured granule speed, assumed constant during the ablation, for a number of granule injection events from four different discharges.

Among the species tested, Li provides the shallower penetration, with most of the granules fully ablated within 4 cm from the separatrix. As indicated by the vertical lines, this is approximate location of the top of the pedestal pressure for these IBS, suggesting that Li 0.7 mm has a good potential for ELM triggering [10].

Carbon and B_4C, when not shattering, appear to penetrate much deeper in the plasma. Indeed experimentally it was found that Li was the only granule type that reliably triggered ELMs and increased the ELM frequency. Conversely, high frequency carbon injection resulted in low triggering efficiency and an effective decrease of frequency of type-I ELMs, likely due to the reduced pedestal pressure by

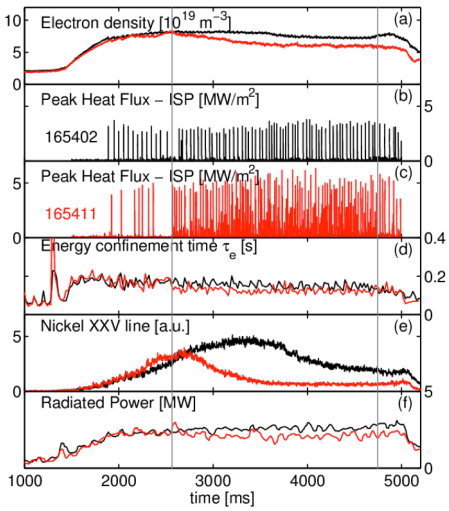

FIG. 5. Evolution of selected plasma parameters for two DIII-D plasmas, with (red) and without (black) Li granule injection.

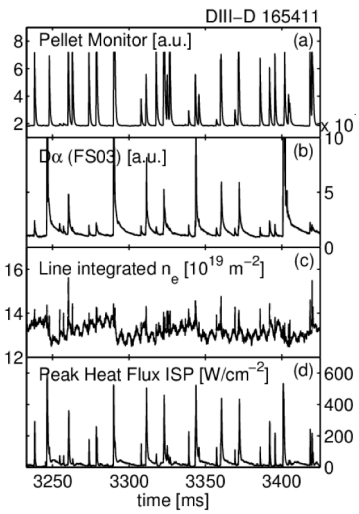

FIG. 6. Example of Li ablation monitor trace compared with various ELM observables.

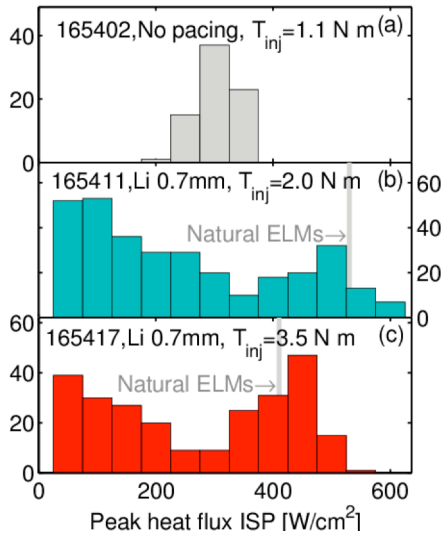

FIG. 7. Distribution of q_{peak} at the ISP, for a reference discharge and two discharges with Li injection.

dilution and a reduced net input power, due to the high ionization energy. Periodic, transient back transitions to L-mode were also observed for injections of 0.6 mm carbon granules at rates >100 Hz. Injection of B_4C resulted in an inconsistent ELM activity, due to the variability of granule size and penetration depth, leading to irregular discharge evolutions.

In the following we focus on results of ELM pacing and mitigation obtained with Li granule injection. Figure 5 shows the evolution of a selection of plasma parameters for a reference discharge in the IBS (T_{inj}=1.5 N-m) and a discharge with injection of 0.6 mm Li granules at ~100 m/s. The Li injection started at t=2.6 s and continued until t=4.8 s, at a constant average rate of 140 Hz. The ELM frequency increased promptly with the Li injection (c). The plasma density gradually decreased from 8 to 6.5x10^{19} m^{-3}. The Ni concentration in the core was strongly reduced indicating a depletion of core metal impurities. This, combined with a lower intrinsic carbon density (not shown), resulted in lower radiative losses, from 4 to 3 MW. Nevertheless, a reduction of energy confinement time was observed in the LGI phase, from τ_E~160 to 140 ms.

By correlating ablation monitor signal with ELM observables, such as D_α and q_{peak} of ISP (Fig. 6) an ~80% ELM triggering probability is found, resulting in an average f_{ELM}~110 Hz, an approximate 4X increase over the natural ELM frequency in the reference discharge with no pacing (25 Hz). However the ELM events triggered appear to combine ELMs of broadly different sizes. In particular the larger ELMs show q_{peak}~500 W/cm^2 [Fig. 6(d)], similar to that observed for natural ELMs, in the same discharge before and after Li injection.

Figure 7 shows the distribution of the q_{peak} observed for the reference discharge and two discharges with increasing Li injection at T_{inj}=2 N-m and 3.5 N-m. In both cases during LGI use, a broad distribution of q_{peak} was observed, where two classes of ELMs can be identified: a class of large ELMs, q_{peak}>300 W/cm2, and a class of smaller ELMs including events with q_{peak} as low as 30 W/cm2. Notice that in this scenario small natural ELMs interleaved with large type-I ELMs are also observed, as for example in the reference discharge for t=2.4-2.6 s. In both LGI discharges the large ELMs are characterized by q_{peak} similar to the natural ELMs in the same discharge. The distinction between small and large ELMs is apparent when considering the heat flux footprint, shown in Fig. 8(a) in terms of wetted area A_q as a function of q_{peak}. Inspection of selected ELMs [Fig.8(b)] shows that large ELMs have heat flux profiles similar to natural ELMs in the same discharge, with the maximum deposition far ~10 cm away from the strike point. Small paced ELMs show a 50% narrower footprint with a clear indication of striations. Considering only the

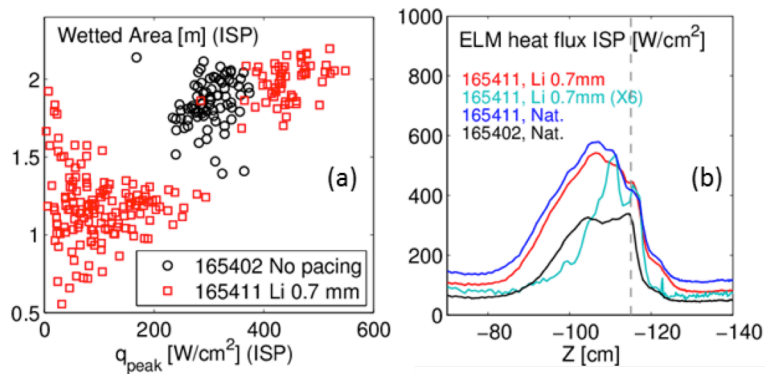

FIG. 8. (a) q_{peak} as a function of ISP wetted area for uncontrolled and Li-paced ELMs. (b) ELM heat flux footprint for selected ELMs. The vertical line indicates the ISP location.

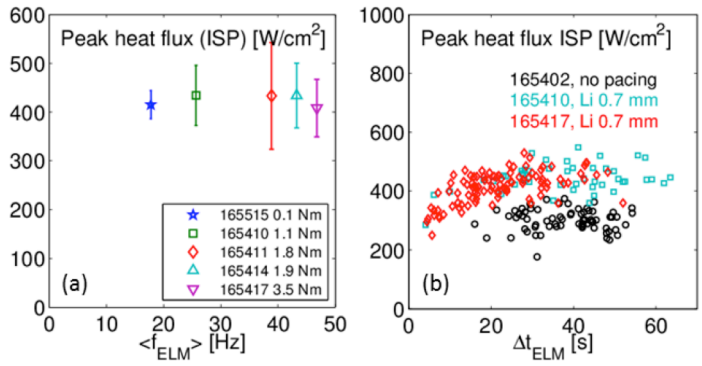

FIG. 9. (a) Average q_{peak} for large ELMs as a function of f_{LE}. (b) q_{peak} measured for large ELMs in three selected discharges, as a function of the pre-ELM period.

occurrence rate of large ELMs (f_{LE}) we find that in the two Li cases in Fig. 7, f_{LE} was respectively 41 Hz and 50 Hz, an approximate 1.5X and 2X increase over the frequency of the large type-I ELMs in the respective reference discharges.

Indeed, when considering a set of plasma experiments at various applied torques T_{inj}=0.05-3.5 N-m, we find that increasing the Li injection frequency up to 140 Hz, resulted in increases of f_{LE} up to 2X, and that the average q_{peak} for large ELMs remained close to 400 W/cm^2, independently from applied torque or f_{LE}. [Fig. 9(a)]. The weak dependence of q_{peak} on ELM frequency is clearly visible in Figure 9(b), where q_{peak} for large ELMs in three selected discharges is shown as a function of the time from the previous large ELM. Possibly due to the non-periodic injection inherent to the IGI [6], large ELMs are observed for a broad range of pre-ELM periods, spanning from 5-50 ms. Over this wide range of periods, q_{peak} is observed not to change significantly. The observations are consistent with a recent report [11], where Li injection of larger size granules (0.9 mm) in the IBS, were discussed: 1) the frequency of large type I ELMs could be increased by a small factor, with most of Li granule injections resulting in smaller ELMs or sub-threshold perturbations; 2) the size of the large ELMs was found to depend weakly on the pre-ELM period.

At present, the mechanism that underlies these results is not understood, especially with reference to the effective mitigation documented in [6], albeit in a different scenario. The role of the pedestal parameters in these experiments has been considered. Figure 10 shows a significant increase of $T_{e,ped}$, during Li injection, as a result of the main ion dilution and reduced P_{rad}. Combined with a lower $n_{e,ped}$, a significant reduction of the pedestal collisionality is found from ν^*=1.2 to 0.5. Previous ELM studies [12] showed that lower pedestal collisionality is associated with larger ELM losses, with a larger contribution from conductive losses, i.e. loss of pedestal temperature. Changes of this kind might play a role for the difficulty to reduce heat-flux in these highly lithiated plasmas. On the other hand, the prompt response to Li injection, showing high q_{peak} at the beginning of Li injection indicates that the phenomenon might be associated with the dynamics of ELM triggering, and specific to the type of perturbations induced by Li granules in this scenario (high density, low q_{95}). To that end, non-linear 3D MHD simulations are required, with a spatial

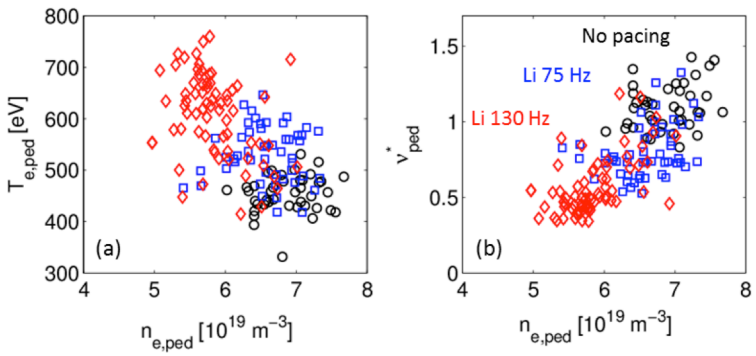

FIG. 10. Pedestal T_e (a) and collisionality ν^* (b) as a function of n_e, for the reference discharge and two discharges with increasing Li injection rate.

resolution able to resolve the fine structure pressure perturbation associated with the granule ablation. A Li injection module has been implemented in the MHD code M3D-C[1] [13], which includes a first principle Li ablation model valid for the experimentally relevant granule sizes [14]. The module has been successfully benchmarked [15], and non-linear 3D simulations on DIII-D equilibria are in progress.

4. Discussion and Outlook

The dataset collected shows that, as the injection frequency is increased to high levels over the natural ELM frequency, indirect effects on pedestal profiles through wall recycling and divertor conditions become important, and might determine the effectiveness of pacing and level of mitigation obtained, thus complicating the interpretation of the results. In the D2P cases illustrated, when injecting at the highest available frequency of 90 Hz, the increase of pedestal collisionality and neutral density in the lower divertor, favors the triggering of small, frequent ELMs and results in extremely favorable mitigation of the ELM peak heat flux. In the case of Li injection, the lower collisionality resulting from lower density and main ion dilution, favors the occurrence of larger and more conductive ELMs. These elements, in many ways specific to the experimental conditions of DIII-D, complicate the extrapolation to the ITER environment. While progress is being made towards the study of the conditions for efficient on-demand ELM triggering with simulation MHD codes like JOREK [10] and M3D-C[1], an accurate prediction should also address the changes of pedestal parameters, SOL characteristics and strike point conditions, which at the highest injection rates may strongly affect the effectiveness of the ELM mitigation.

5. Acknowledgment

This material is based upon work supported by the U.S. Department of Energy, Office of Science, Office of Fusion Energy Sciences, using the DIII-D National Fusion Facility, a DOE Office of Science user facility, under Awards DE-AC02-09CH11466[1], DE-AC05-00OR22725[2], DE-FC02-04ER54698[3], DE-FG02-06ER54867 and DE-AC52-07NA27344[4]. DIII-D data shown in this paper can be obtained in digital format by following the links at https://fusion.gat.com/global/D3D_DMP.

6. References

[1] A. LOARTE *et al.*, *Nuclear Fusion*, 54(3):033007 (2014).
[2] P.T. LANG *et al.*, *Nuclear Fusion*, 44(5):665 (2004).
[3] L.R. BAYLOR *et al.*, *Phys. Rev. Lett.*, 110:245001, Jun (2013).
[4] R. MAINGI *et al.*, *Nuclear Fusion*, 54(11):114016 (2014).
[5] D.K. MANSFIELD *et al.*, *Nuclear Fusion*, 53(11):113023 (2013).
[6] A. BORTOLON *et al. Nuclear Fusion*, 56(5):056008 (2016).
[7] E.J. DOYLE *et al. Nuclear Fusion*, 50(7):075005 (2010).
[8] L.R. BAYLOR *et al.*, *Physics of Plasmas*, 20(8):082513 (2013).
[9] P.B. SNYDER *et al.*, *Physics of Plasmas*, 9(5):2037–2043 (2002).
[10] S. FUTATANI *et al.*, *Nuclear Fusion*, 54(7):073008 (2014).
[11] A. BORTOLON *et al.*, submitted to *Nuclear Materials and Energy* (2016).
[12] A.W. LEONARD, *Physics of Plasmas*, 21(9):090501 (2014).
[13] N.M. FERRARO and S.C. JARDIN, *Journal of Comp. Physics*, 228(20):7742 – 7770 (2009).
[14] P.B. PARKS, to be submitted to *Physics of Plasmas*.
[15] A. FIL *et al.*, submitted to *Nuclear Materials and Energy* (2016).